Journal of Power Sources 379 (2018) 261–269

Contents lists available at ScienceDirect

Journal of Power Sources

journal homepage: www.elsevier.com/locate/jpowsour

Si nanowires/Cu nanowires bilayer fabric as a lithium ion capacitor anode with excellent performance

Chien-Ming Lai[1], Tzu-Lun Kao[1], Hsing-Yu Tuan*

Department of Chemical Engineering, National Tsing Hua University, 101, Section 2, Kuang-Fu Road, Hsinchu, 30013, Taiwan, ROC

HIGHLIGHTS

- A Si nanowires/Cu nanowires bilayer fabric showed a capacitance of 156 F g^{-1}.
- Deliver 68 F g^{-1} at a current density of 20 A g^{-1}.
- Deliver 210 W h kg^{-1} at a power density of 193 W kg^{-1}.
- Deliver 43 W h kg^{-1} at a power density 99 kW kg^{-1}.

GRAPHICAL ABSTRACT

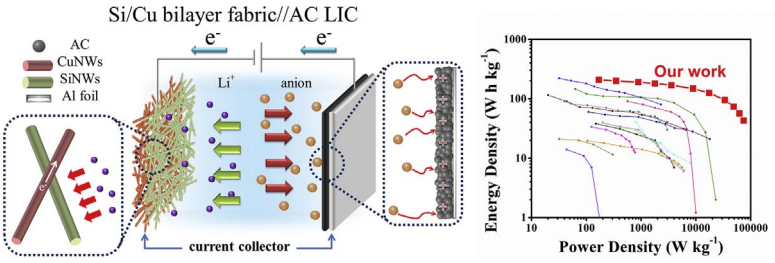

ARTICLE INFO

Keywords:
Si nanowires
Cu nanowires
Pre-lithiation
Bilayer fabric
Lithium-ion capacitor

ABSTRACT

A light and binder-free bilayer fabric electrode composed of silicon nanowires and copper nanowires for lithium-ion capacitors (LICs) is reported. A lithium ion capacitor is proposed employing pre-lithiated silicon/copper nanowire fabric and activated carbon as the anode and the cathode, respectively. These LICs show remarkable performance with a specific capacitance of 156 F g^{-1} at 0.1 A g^{-1}, which is approximately twice of that of activated carbon in electric double-layer capacitors (EDLCs), and still exhibit a fine specific capacitance of 68 F g^{-1} even at a high current density of 20 A g^{-1}. At a low power density of 193 W kg^{-1}, the Si/Cu fabric//AC LIC can achieve high energy density of 210 W h kg^{-1}. As the power density is increased to 99 kW kg^{-1}, the energy density still remains at 43 W h kg^{-1}, showing the prominent rate performance.

1. Introduction

Capacitors are energy storage devices that can provide high power density and long cycle life, but suffered from low energy density, limiting the diversity of the possible applications of capacitors [1–3]. Hence the birth of lithium ion capacitors (LICs), also called lithium ion hybrid supercapacitors, promotes the performances to a whole new level. LICs are newly developed energy storage devices composed of one lithium ion battery (LIB)-type electrode and one capacitor-type electrode in the organic electrolyte with lithium ion salt to deliver both high energy density and high power density with long cycle life [4–6]. In fact, the replacement of one of the carbonaceous electrodes in the capacitors with Li-storing electrode not only doubles the theoretical specific capacitance, but also elevates the operating voltage from 2.7 V to 4.2 V, leading a higher energy density around 4–5 times of the original value.

A typical reaction within a LIC involves the adsorption/desorption of PF_6^- at the capacitor-type electrode and the reactions between lithium ions and the LIB-type electrode [7]. Currently, the common capacitor-type electrode is usually made of carbonaceous materials with high surface area, such as activated carbon (AC) [8,9], graphene [10], and carbon nanotube [2]. On the other hand, the LIB-type electrode materials are those able to intercalate or alloy with lithium ions, including carbonaceous materials, intercalation compounds, and metal

* Corresponding author.
E-mail address: hytuan@che.nthu.edu.tw (H.-Y. Tuan).
[1] These authors contributed equally to this work.

https://doi.org/10.1016/j.jpowsour.2018.01.046
Received 1 May 2017; Received in revised form 11 January 2018; Accepted 18 January 2018
Available online 03 February 2018
0378-7753/

oxides. In the incipient studies of LICs, lithium-contained metal oxide compounds like $LiNi_{0.5}Mn_{1.5}O_4$ [11,12], $LiFePO_4$ [13], and $LiMn_2O_4$ [14], were employed as the anode. In 2001, Amatucci et al. reported the first case of an energy storage cell with the same conformation of LICs utilizing $Li_4Ti_5O_{12}$ and activated carbon as the anode and the cathode, respectively, showing good cycle life with the capacity loss less than 6% over 4000 cycles between 1.5 V and 2.5 V [15]. Du Pasquier et al. bettered the capacitance of this device to 500 F with an energy density of 11 W h kg^{-1}, a power density of 800 W kg^{-1} [16], and a prolonged cycle life over 10,000 cycles, suggesting hybrid supercapacitors possessed great potential for numerous automotive applications.

In addition, an even higher energy density can be achieved by substituting other materials with closer potential to lithium for those lithium-contained metal oxide compounds. Intuitively, pre-lithiation would be an effective way to lower the potential of the anode to be lithium metal-like, resulting in a widened operating voltage window. Moreover, careful pre-lithiation would lead to the formation of compact solid electrolyte interface (SEI) layers, which were beneficial for the electrochemical performances, resulting a better cycling life and higher energy density. Zhang et al. developed an iron oxide/graphene nanocomposite as the anode material, of which the capacity was over 1000 mA h g^{-1} [7]. The LIC was assembled with pre-lithiated iron oxide/graphene nanocomposite and 3D graphene as the anode and the cathode, respectively, exhibiting energy densities ranging from 204 to 65 W h kg^{-1} as the power density increased from 55 to 4600 W kg^{-1}, which was much higher than most lithium ion capacitors ever reported before.

Silicon (Si) possessing the highest theoretical specific capacity of 3579 mA h g^{-1} [17–20], is a low-priced and earth-abundant element studied as the anode material of LIBs in considerable reports [21,22]. Yet, only a handful of studies introduced Si into LICs, for instance, B-Si/SiO_2/C//AC LIC exhibited ordinary energy density from 89 to 128 W h kg^{-1}, power density from 1.2 to 9.7 kW kg^{-1}, and a 70% retention when cycled at 1.6 A g^{-1} for 6000 cycles, which was reported in 2014 [23,24]. The near-lithium reaction plateau leads to a wider voltage window, which is advantageous for LICs achieving a higher energy density. Here, we investigate Si as the anode of LICs, which were assembled by employing the pre-lithiated Si/Cu bilayer fabric and AC as the anode and the cathode, respectively. We found that the Si/Cu bilayer fabric anode, which was a binder-free electrode, could provide a large surface area for sufficient contacts with the electrolyte, a high electrical conduction, and a large space available to tolerate volume change, which can potentially improve the cycling stability and the rate capability and promote the electrochemical performances toward the top-right region of the Ragone plot. Scheme 1 shows the schematic mechanism of the Si/Cu nanowires bilayer fabric//AC LIC and its possible application. The specific capacitance achieves 156 F g^{-1} at a current density of 0.1 A g^{-1}, and still remains at 68 F g^{-1} at a high current density of 20 A g^{-1}. Additionally, the long cycle stability is the admirable quality of Si/Cu fabric//AC LIC. After 1500 cycles, the LIC shows a specific capacitance of 60 F g^{-1} at a current density of 5 A g^{-1}. As a result, the energy density is improved to 210 W h kg^{-1}, and yet remains at a fine value of 43 W h kg^{-1} at an ultrahigh power density of 99 kW kg^{-1}.

2. Experimental section

2.1. Materials

All reagents and solvents were used as received. Oleylamine (OLA, $C_{18}H_{37}N$, 70%), anhydrous toluene ($C_6H_5CH_3$, 99.99%), chloroform ($CHCl_3$, 99.8%), ethanol (C_2H_5OH, 99.8%), hexanes (C_6H_{14}, 98.5%), methanol (CH_3OH, 99.8%), 1-dodecanethiol ($C_{12}H_{26}S$, 98%), hydrochloric acid (HCl, 37 wt%), diethyl carbonate (DEC, $C_5H_{13}O_3$), bis(bis(trimethylsilyl)amino)tin ($Sn(HMDS)_2$), poly acrylic acid(PAA, Mw 450,000) were purchased from Sigma-Aldrich. Copper chloride (CuCl, 99.99%) was purchased from Alfa. Phenylsilane (MPS, $C_6H_5SiH_3$) was purchased from Gelest. Lithium hexafluorophosphate ($LiPF_6$), fluoroethylene carbonate (FEC, $C_3H_3FO_3$), electrolyte (1 M $LiPF_6$ in mixture of ethyl carbonate (EC) and dimethyl carbonate (DMC) with volume ratio of 1:1), polyvinylidene fluoride (PVDF, -$(C_2H_2F_2)_n$-), N-methyl-2-pyrrolidone (NMP, C_5H_9NO), Super P carbon black, lithium metal foil, copper metal foil, aluminum metal foil, Celgard membrane, coin-type cells (CR2032) were purchased from Shining Energy Corp. Activated carbon was purchased from China Steel Chemical Corp.

2.2. Synthesis of silicon nanowires

Sn-seeded Si nanowires were synthesized by supercritical fluid-liquid-solid (SFLS) method with the presence of tin as the seed. The 10 ml titanium reactor was first put into an argon-filled glovebox to assure the inert environment inside the reactor, and then was sealed and brought out from the glove box. The reactor was covered with heating tape with the temperature kept at 490 °C. The inlet of the 10 ml reactor was connected to a six-way valve (valco) equipped with a 5 ml injection cylinder *via* stainless steel high-pressure (1/1600 i.d.) tubing. A high pressure liquid chromatography (HPLC) pump (Lab Alliance, series 1500) in series to the six-way valve was employed to pressurize the reactor as well as to deliver the reactant solution from the injection cylinder into the reactor with pressure monitored by a digital pressure gauge (Yan-Chang Technology). The reactant solution was prepared in the glove box. In a typical Sn-seeded Si nanowires synthesis, 250 μL MPS, 36 μL $Sn(HMDS)_2$, and 4.75 ml anhydrous toluene were well-mixed and loaded to the 5 ml injection cylinder after the reactor was heated to reaction temperature (490 °C) and pressurized to 6.2 MPa. The reactant mixture, of which the molar ratio of Si to Sn is 22:1, was fed to the reactor at a flow rate of 0.5 ml min^{-1} for 15 min. The HPLC pump was turned off afterward, and the reactor was removed from the system and submerged in a water bath until it reached room temperature. The product was collected and then centrifuged with a mixture of chloroform, toluene, and ethanol at a volume ratio of 1:1:1 at 8000 rpm for 5 min thrice to remove the byproducts. The resulting solid product was dried and immersed in 10% HCl for 15 min to remove all the tin within the product, followed by rinsing it with methanol to remove the residue HCl thoroughly [25]. Furthermore, the Si nanowires were passivated with 1-dodecanethiol to improve the dispersity of Si nanowires in organic solvents and the oxidation resistance [26,27]. The Si nanowires were placed in a 20 ml sample vial, followed by the addition

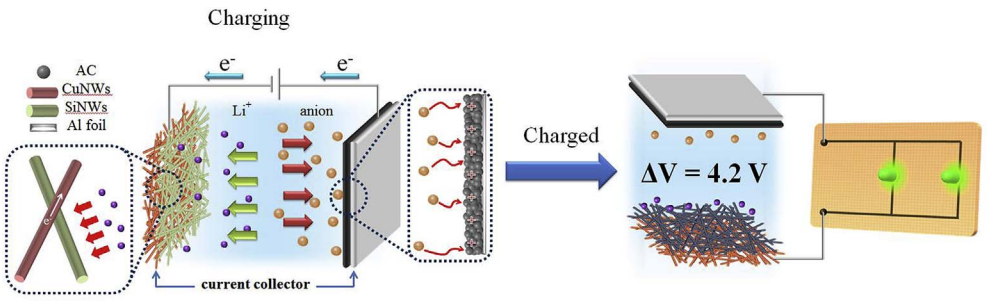

Scheme 1. The schematic mechanism of the Si/Cu nanowires bilayer fabric//AC LIC and its application.

of 15 ml 1-dodecanethiol. The vial was heated and kept at 80 °C under argon atmosphere with continuous vigorous stirring for 12 h. After the thiolation of Si nanowires finished, the solid product was precipitated and washed by centrifugation with a mixture of toluene and methanol at a volume ratio of 1:1 to remove excess 1-dodecanethiol. Finally, Si nanowires were put into a 20 mL sample vial and stored in the argon-filled glovebox for further uses.

2.3. Synthesis of copper nanowires

For Cu nanowires synthesis, 0.3 g CuCl and 30 mL OLA were added into a 50 mL three-necked flask in the glovebox. The flask was then connected to the Schlenk line with one side-neck sealed by a rubber septa and the other by a thermocouple. The system was purged by a continuous argon flow for the removal of oxygen. Then, the flask was heated to 110 °C and kept for 50 min for the removal of water. At last, the three-necked flask was heated to 250 °C and kept for 50 min. Meanwhile, it could be clearly observed that the color of the solution changed from bright yellow to red. After the reaction completed, the Cu nanowires were removed from the three-necked flask and washed by centrifugation with hexane for several times. The Cu nanowires were put into the sample vial and stored in the glovebox for further uses.

2.4. Preparation of bilayer Si/Cu nanowire fabric electrode

Si nanowires and Cu nanowires were dispersed in toluene and hexane, respectively. First, the Cu nanowires dispersion was dropcasted into the Teflon mold (1 cm × 1 cm). The Si nanowires dispersion was then dropcasted into the Teflon mold after the hexane was fully evaporated. When all the toluene completely evaporated, the upper part of the Teflon mold was lifted, and the layered Si/Cu nanowire fabric was freed and annealed at 500 °C under hydrogen and argon flow. Finally, the Si/Cu nanowires fabric was stored in the glovebox for further uses. Typically, the mass loading of silicon in the bilayer fabric is around 0.5 mg, and it's easily tunable.

2.5. Preparation of activated carbon electrode

The electrode was prepared by mixing 70% activated carbon (AC), 20% super P carbon black, and 10% polyvinylidene fluoride (PVDF) in weight percentage in N-methyl-2-pyrrolidinone (NMP) solvent forming a homogeneous slurry. Then, the slurry was spread onto aluminum foil by automatic coating machine to assure the uniformity of the electrode thickness. The electrodes were dried at 60 °C in oven for 1 day and then 120 °C under argon for the removal of residual water. After the rolling press treatment, the electrode was tailored to rounded shape with a diameter of 11 mm. The AC electrode was stored inside the glovebox for further uses. The mass loading of AC on the electrode is easily tunable with a 0.2 mg–3 mg range by adjusting the slurry concentration and the thickness, and the mass loadings of AC are listed in Table S1.

2.6. Characterization

Both the silicon and copper nanowires were characterized by means of scanning electron microscopy (SEM), transmission electron microscopy (TEM), energy-dispersive X-ray spectroscopy (EDS), and X-ray diffraction (XRD). The high-resolution SEM images of Si and Cu nanowires were obtained utilizing a HITACHI-SU8010 field-emission SEM with 10 kV accelerating voltage and 8 mm working distance. The TEM samples were prepared by drop casting the dispersion of silicon or copper nanowires in toluene onto 300 mesh lacey carbon-coated copper grids, which were later dried in an oven under vacuum overnight. High-resolution TEM images and selected area electron diffraction (SAED) were obtained by JEOL ARM200F. Meanwhile, EDS was carried out for elemental analysis of Sn-seeded Si nanowires with as-prepared sample on copper grids. XRD patterns were procured by a Rigaku Ultima IV X-ray diffractometer with Cu target generating Cu Kα radiation (λ = 1.54 Å) as the source of X-ray.

2.7. Half-cell lithium-ion battery and lithium-ion capacitor assembly and electrochemical characterization

The anode electrode of the half-cell lithium-lon battery was Si/Cu nanowires fabric with the mass loading around 1 mg/cm [2] of Si nanowires and 3 mg/cm [2] of Cu nanowires. Si/Cu nanowires electrode, microporous polyethylene separator wetted by the electrolyte composed of 1 M $LiPF_6$ in EC/DEC 1:1 (v:v) with extra 5% FEC, and lithium metal foil were assembled in this order within a CR2032 coin cell inside the glovebox. Electrochemical performance of the Si/Cu nanowires electrode was evaluated between 0.01 V and 1.5 V on Maccor Series 4000 instruments.

Before the lithium-ion capacitor assembly, the Si/Cu nanowires electrode is prelithiated at a current density of C/20. Then, the Si/Cu nanowires electrode was removed from the cell and fully dried for the following LIC assembly. The activated carbon electrode was used as cathode with 0.3 mg/cm^2 of activated carbon loaded on it. Prelithiated Si/Cu nanowires electrode, microporous polyethylene separator wetted by the 1 M $LiPF_6$ in EC/DMC 1:1 (v:v) electrolyte, and the activated carbon electrode were assembled in this order in a CR2032 coin cell in the glovebox. Electrochemical performance of the LIC was tested between 1.5 V and 4.2 V on Biologic VMP3 instruments.

The values of the specific capacitance (C, unit: F g^{-1}), energy density (E, unit: W h kg^{-1}), and power density (P, unit: W kg^{-1}) were all calculated from the discharge curves by these three questions shown below:

$$E = 1000 \times \int_{t_1}^{t_2} IVdt = 1000 \times I \int_{t_1}^{t_2} Vdt$$

$$C = 2 \times 3.6 \times E/(V_{max}{}^2 - V_{min}{}^2)$$

$$P = E/t\ ,$$

where I (A g^{-1}) is the discharge current density based on the mass of active materials and is constant in each cycle, t (h) is the discharge time, Vmax (V) is the maximum voltage during discharging and Vmin (V) is the minimum voltage during discharging. Although the capacitance and the power density of a LIC is not constant over the voltage window or time, we can still obtain an average capacitance and power density that can represent the electrochemical performance of the LIC by invoking the equations above. Detailed integration is shown in supporting information.

3. Results and discussion

The Sn-seeded Si nanowires were synthesized *via* the supercritical fluid-liquid-solid (SFLS) route with the 22:1 molar ratio of Si to Sn. Described in the previous studies [28], MPS went through bimolecular disproportionation by phenyl redistribution resulting in the formation of silane and higher order phenylsilane The generated Si from the decomposition of the silane dissolved into the Sn particles and crystallized into nanowires [29]. Figure S1(a,b) shows the scanning electron microscopy (SEM) and the transmission electron microscopy (TEM) images of the as-synthesized Sn-seeded Si nanowires, indicating the average diameter of the Si nanowires is in the proximity of 20 nm and the length around 25 μm. The sharp peaks in the X-ray diffraction (XRD) spectrum shown in Figure S1(c) suggest good crystallinity of the Si nanowires, and can be perfectly indexed to the face-centered cubic Si (JCPDS no.89-5012) with the presence of crystalline Sn (JCPDS no.89-4898). In addition, energy-dispersive X-ray spectroscopy (EDS) was used to analyze the composition of the Si nanowires (Figure S2), showing Sn exists only in the tip but not in the wire, which supports the statement we claimed regarding the growth mechanism of the Si

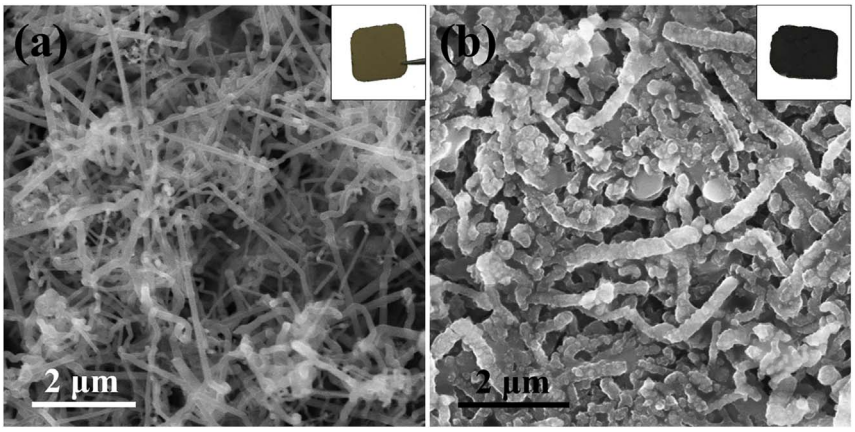

Fig. 1. SEM images of the Si/Cu bilayer fabric on the silicon side (a) before lithiation (b) after lithiation. The insets are the corresponding photos. (For interpretation of the references to color in this figure legend, the reader is referred to the Web version of this article.)

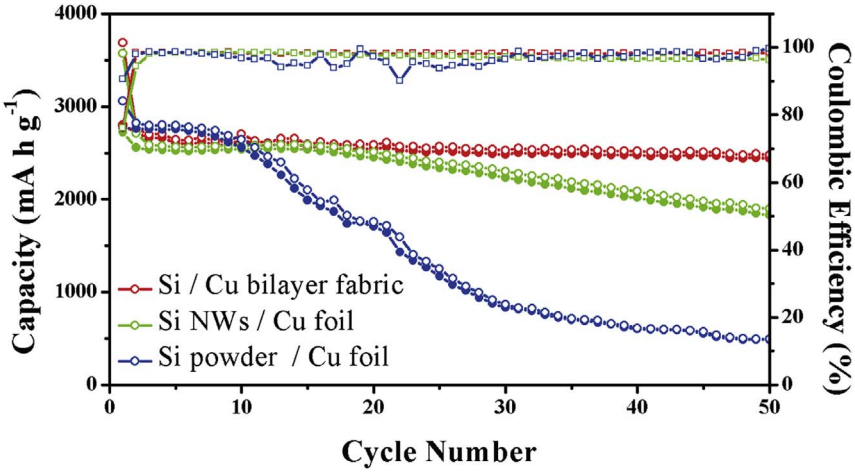

Fig. 2. Cycling performances of Li-ion half cells using silicon as the active material and copper as the current collector in three different cases at a slow C rate of 0.1 C: Si/Cu bilayer fabric, Si nanowire on Cu foil, and Si powders on Cu foil. (For interpretation of the references to color in this figure legend, the reader is referred to the Web version of this article.)

nanowires. Inevitably, Sn particles were removed by simple treatment in HCl for 15 min, which is evidenced by the XRD spectrum (Figure S3(a)) and the SEM image (Figure S3(b)), assuring that the lithiation reaction is solely attributed to the Si nanowires. Furthermore, the Si nanowires were single-crystalline as confirmed by the high-resolution TEM image (Figure S3(c)), which showed clear lattice fringes. Other than showing the single-crystalline nature, the corresponding selected-area electron diffraction pattern with a zone axis of [1 1 1] also indicates the Si nanowire grew along [1 1 2] direction. On the other hand, Cu nanowires were synthesized by reacting CuCl with oleylamine according to the previous study [30]. The SEM images (Figure S4(a,b)) shows the Cu nanowires with an average diameter of 55 nm and length up to 30 μm. The crystallinity was identified by means of XRD with the spectrum in close agreement with face-centered cubic Cu (JCPDS no.89-2838) in Figure S4(c). Moreover, the single crystallinity of the Cu nanowires is observed from the high-resolution TEM image (Figure S4(d)), showing the Cu nanowires grew along the [1 1 0] direction and a lattice spacing of 0.13 nm corresponding to the (2 2 0) lattice plane.

The 1 cm × 1 cm squares of Si/Cu bilayer fabric electrode composed of densely entangled nanowires was prepared by drop-casting concentrated dispersions of nanowires in toluene into a Teflon mold. It is instantaneously recognized that all nanowires are well-interlaced with each other in the SEM image (Fig. 1(a)). The anode was treated with pre-lithiation to obtain a widened operating voltage window and compact SEI layer on the surface of the electrode, leading a LIC with prolonged cycle life and an elevated energy density. SEM images of the Si nanowires before and after lithiation (Fig. 1(a and b)) show that the morphology nearly retains without any damage of cracking while the average diameter of the pre-lithiated Si nanowires is widened from ~20 to ~150 nm, indicating that Si nanowires become an alloy with lithium and the SEI layer forms on the surface.

To systematically assess the quality of the electrodes in the LICs we report here, the performances of anode and cathode of this LIC were tested separately prior to the evaluation of as-assembled LICs. As to the cathode, activated carbon-based EDLCs were established and tested at different current densities (Figure S5), showing good quality. As to the anode, multiple types of silicon-based half-cell LIBs were constructed and evaluated with charge/discharge galvanostatic cycles between 0.01 V and 1.5 V. The additional FEC we added could help grow a proper and compact solid-electrolyte interface (SEI) layer on the surface of the electrode. The specific capacity of Si/Cu fabric is 2800 mA h g^{-1} (Fig. 2) when cycled at 0.1 C, which is much higher compared to the respective performances of Si powder and Si nanowires on the Cu foil. Si/Cu fabric shows a stable capacity of 2500 mA h g^{-1} with over 98% Coulombic efficiency during 50 cycles at a slow rate of C/10, which is higher than Si powders (500 mA h g^{-1}) and Si nanowires (1900 mA h g^{-1}) on the Cu foil. Additionally, Si/Cu nanowire fabric displays a fine capacity of 900 mA h g^{-1} when cycled at an increased rate of 1C (Figure S6(a)). The discharging profile (Figure S6(b)) reveals a clear reaction plateau at 0.2 V for lithium intercalation as the deintercalation occurs at 0.25 V observed in the charging profile with the current density ranging from C/10 to 1C. With this superior performance, we supposed that Cu nanowires are well-contacted with Si nanowires and acted as a perfect current collector. Ultimately, LICs were fabricated by combining the activated carbon-based cathode and one of those silicon-based anodes for evaluation. Fig. 3(a) shows the cycle performance of the LICs applying AC with the three pre-lithiated electrodes in the voltage window from 1.5 V to 4.2 V, and Fig. 3(b) is converted from Fig. 3(a) to see the relation between capacitance and current density clearly. The capacitance of Si/Cu fabric//AC LICs is

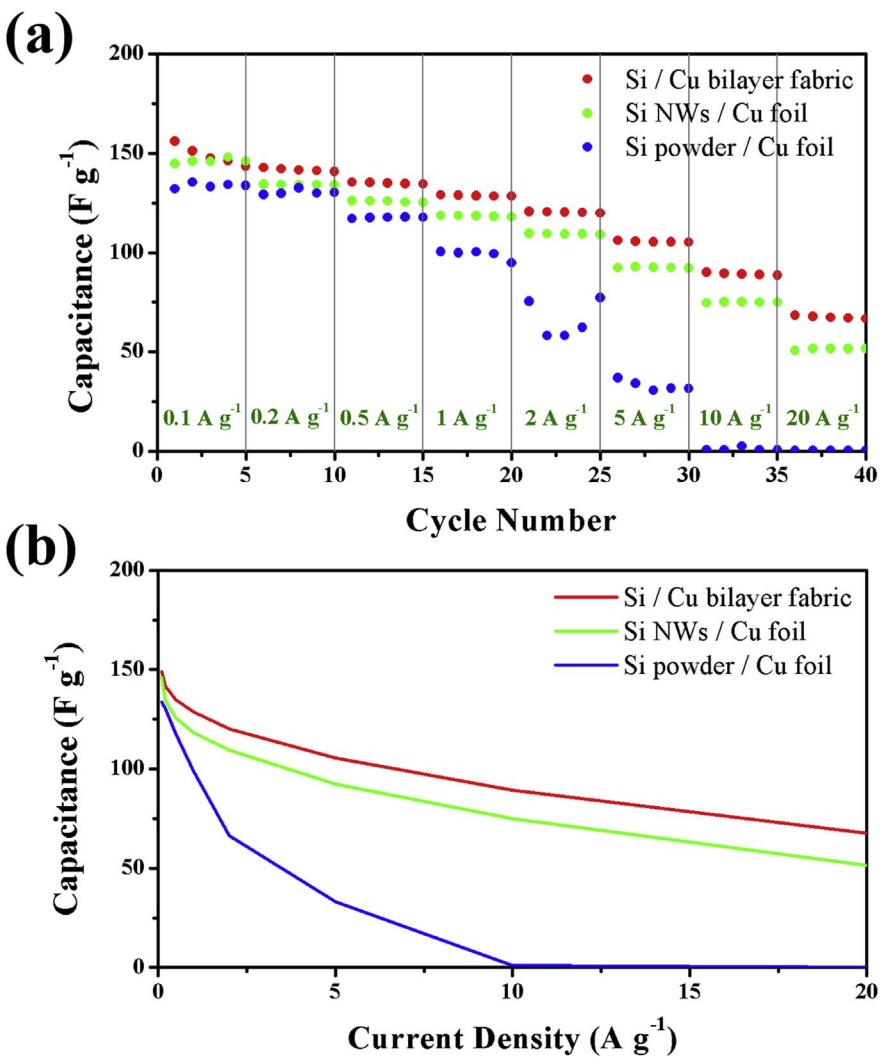

Fig. 3. Electrochemical performances of LICs using silicon as the active material and copper as the current collector in three different cases: Si/Cu bilayer fabric, Si nanowire on Cu foil, and Si powders on Cu foil. (a) Rate capability of lithium ion capacitors from 0.1 A g^{-1} to 20 A g^{-1}. (b) Specific capacitance in different current density from 0.1 A g^{-1} to 20 A g^{-1}. (For interpretation of the references to color in this figure legend, the reader is referred to the Web version of this article.)

156 F g^{-1} at a current rate of 0.1 A g^{-1}, which is higher than those of Si powder (132 F g^{-1}) and Si nanowires (145 F g^{-1}) on Cu foil. Even at a high current density of 20 A g^{-1}, the specific capacitance of LIC using the bilayer fabric electrode still remains 68 F g^{-1}. Such remarkable properties of Si/Cu nanowire fabric in cycle stability and rate capability make it a superior candidate of lithium ion capacitor with better energy density and power density.

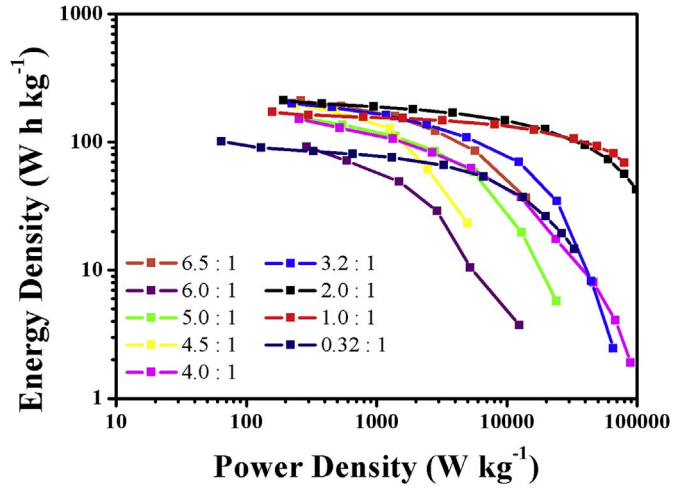

Fig. 4. Ragone plot of the LICs with different mass ratios of AC to silicon. (For interpretation of the references to color in this figure legend, the reader is referred to the Web version of this article.)

It is inevitable to reach a best compromise between energy and power considering that capacitors are likely used as a power device, therefore, the influence of the mass ratio of AC to Si is investigated and presented in Fig. 4, showing the performances with the mass ratio from 0.32 to 6.5. At the ratio of 2.0, it's clear that the lithium ion capacitor achieves the highest power density of 99,000 W kg^{-1} while the energy density maintains at a fine value when cycled at increased charging/discharging rates. In addition, the CV curves were measured in various scan rates (Fig. 5(a)). Different from the symmetric supercapacitor, the shapes of the CV curves of the LICs were not exactly rectangular. As far as we're concerned, the near-rectangular shape in CV plot was extremely normal in LICs, even sharp peaks representing the reaction of lithium ion batteries could be observed in some cases [7,31,32]. We concluded that it sufficed to say that the Si/Cu//AC LICs we reported here could be categorized as hybrid electrochemical capacitor. Furthermore, the higher current density is tested for Si/Cu fabric//AC LIC in Fig. 5(b). At the high current density of 30, 40, and 50 A g^{-1}, the capacitance still remains at 98, 89, and 69 F g^{-1}. The charge/discharge profiles clearly shows near-triangular shape with no platform in the voltage window of 1.5–4.2 V, indicating the Si/Cu fabric//AC lithium ion capacitor behaves capacitively (Fig. 5(c and d)). The IR drop of LICs shown in Fig. 5(d) was frequently observed in many previous studies, and it was inevitable due to the battery component [33–36]. Especially

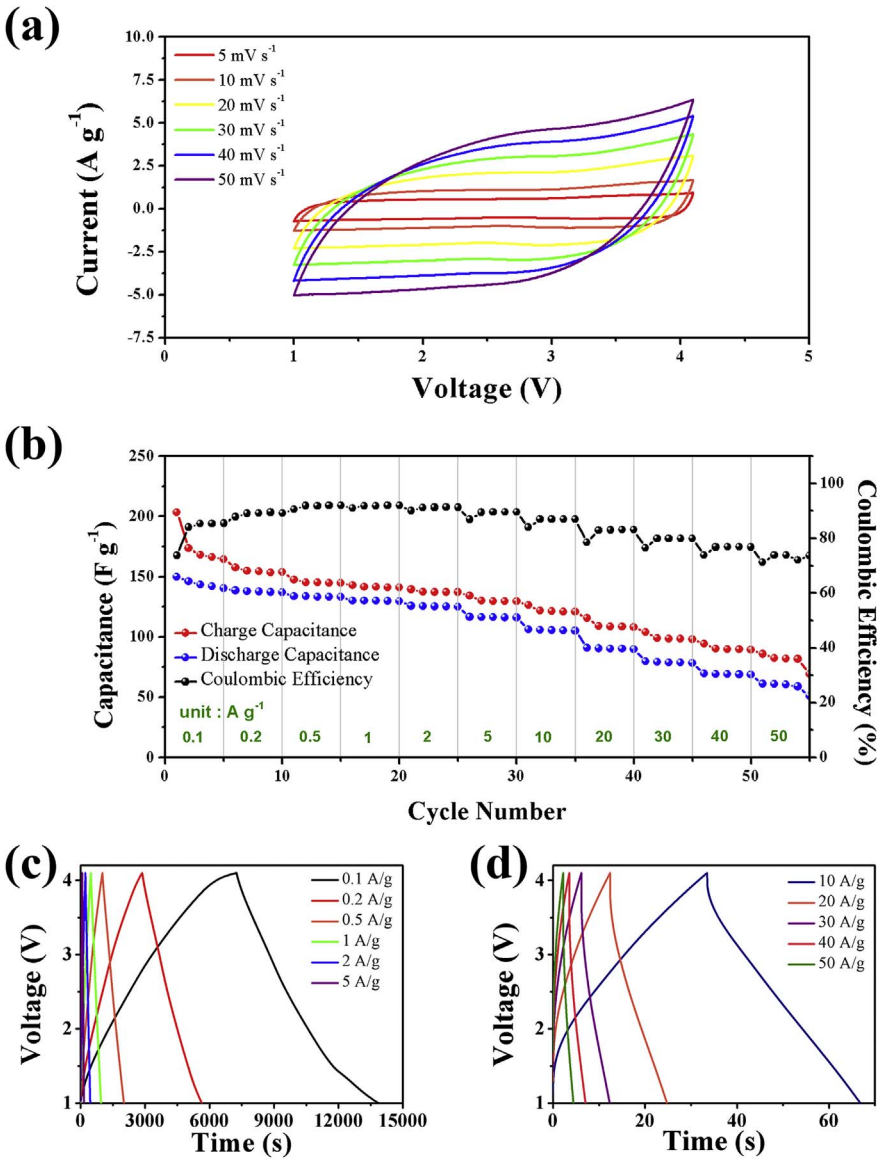

Fig. 5. Electrochemical performance of Si/Cu fabric//AC lithium ion capacitors with the AC/Si mass ratio of 2: (a) CV profiles of LIC scanning from 5 mV s^{-1} to 50 mV s^{-1} (b) Rate capability of the LIC from 0.1 A g^{-1} to 50 A g^{-1} (c–d) Voltage profiles of the LIC from 0.1 A g^{-1} to 50 A g^{-1}.

when applying an increased current rate, the IR drop would become more obvious.

Si/Cu fabric//AC lithium ion capacitor also exhibits long-term cycling stability. In Fig. 6(a), the cycling performance tests 1500 cycles at a constant current density of 5 A g^{-1}. The capacity remains 60 F g^{-1} with near 70% coulombic efficiency, whose retention is as high as 54% after 1500 cycles with an AC to silicon mass ratio of 2:1. In this design, AC is the limiting reagent despite the mass ratios we employed because of the high capacity of silicon (3579 mA h g^{-1}), which indicates only partial silicon reacts during cycles, and this is probably why our LICs exhibit long cycling life despite that silicon is known for short cycling life, resulting from its volume expansion during cycles. The characteristic linear charge/discharge curves in Fig. 6(b) suggest that the AC electrode undertake a non-Faradaic capacitive reaction which is merely adsorption and desorption on the surface. EIS measurements are executed to evaluate the electrical conduction and the Li^+ diffusion process to assess the quality of the whole lithium ion capacitor. The Nyquist plots before cycling and after cycling are shown in Fig. 6(c). The high-frequency semicircle is assigned to the charge-transfer impedance of the electrode/electrolyte interface, reflecting two processes: anions adsorbing/desorbing onto/from the surface of cathode and Li ions passing through from the electrolyte to the surface of anode. The linear section corresponds to the Li diffusion process inside the electrodes, revealing the Li ions intercalate/deintercalate at the anode. The semicircles clearly indicate that the transfer resistance increases with cycling. Additionally, the impedance in both real and imaginary parts are larger than that before cycling, which can be attributed to the increased resistance in the diffusion and migration pathways of the electrolyte ions. In our other attempt using more SiNWs (AC/Si = 0.32) in the Si/Cu fabric//AC LIC, the cycling performance is tremendously bettered, showing a higher retention of 90% with an extremely more lasting cycle life of 30,000 cycles when cycled at an even higher current density of 10 A g^{-1} (Fig. 6(d)), which is foreseeable as the result of the increased usage of silicon in this asymmetrically-designed LIC, implying an increased quantity of active sites, hence the lengthened cycling life. Fig. 6(e) shows the SEM image of the SiNWs which experienced long cycling test, and the morphology of the SiNWs remains nearly intact, which is in accordance with the observed long-term cycling stability. A single coin cell was demonstrated powering up green LED bulbs (Fig. 6(f)). This LIC provided higher voltage and better energy density than supercapacitors, which couldn't turn on the green LED bulbs. In addition, the LIC was repeatedly charged in 1 min and then used to illuminate the LED bulbs to present both high power density and high energy density.

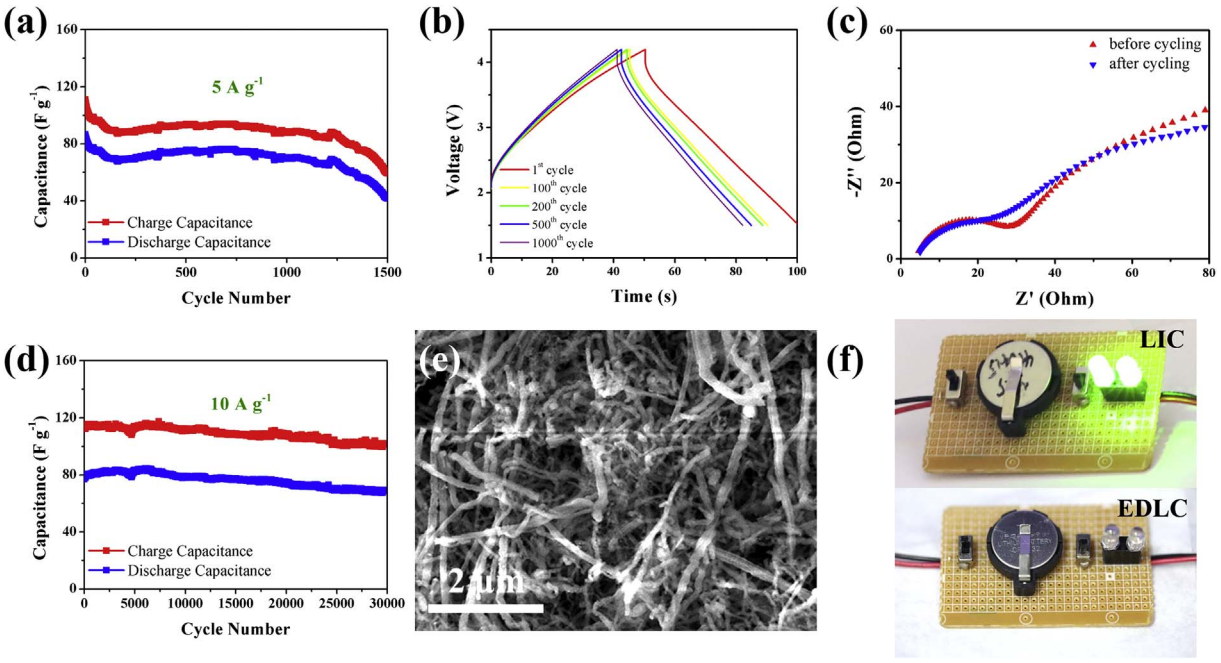

Fig. 6. (a) Cycling performance of the LIC with the AC/Si mass ratio of 2 at 5 A g^{-1} (b) The corresponding voltage profiles of the LIC before cycling and after cycling (c) The corresponding electrical impedance spectra (EIS) before and after cycling (d) Cycling performance of the LIC with the AC/Si mass ratio of 0.32 at 10 A g^{-1} (e) The SEM image of Si/Cu bilayer fabric on the silicon side after cycling for 30,000 cycles at 10 A g^{-1} (f) Demonstration of Si/Cu fabric//AC LIC lighting up two green LED bulbs. (For interpretation of the references to color in this figure legend, the reader is referred to the Web version of this article.)

The Ragone plot (energy density vs. power density) is illustrated in Fig. 7, of which the calculations of the energy density and the power density are based on the total mass of active materials in both electrodes, and all the detailed information on this figure is given in Table 1. It is obvious that the performances of the Si/Cu fabric//AC LIC are the best compared to other reported LICs considering both energy density and power density. The Si/Cu bilayer fabric anode provides a large surface area for sufficient contacts with the electrolyte, a high electrical conduction, and a large space available to endure volume change, which leads to good cycling stability and excellent rate capability and pushes the electrochemical performances toward the top-right region of the Ragone plot. At a low power density of 193 W kg^{-1}, the Si/Cu fabric//AC LIC can achieve high energy density of 210 W h kg^{-1}. As the power density is increased to 99 kW kg^{-1}, the energy density still remains at 43 W h kg^{-1}, showing the prominent rate performance. With the previous experience of the Ge/Cu fabric LIBs anode we recently reported [48], the great high-rate performance of this Si/Cu fabric//AC LIC can be attributed to the entanglement of the two layers of nanowires at the interface, which not only creates strong wire-to-wire adhesion that prevents the detachment of the active material, but also provides better electrical conduction, resulting from the two layers of nanowires penetrating into each other instead of a clean boundary. Hence, the bilayer Si/Cu nanowire fabric is a perfectly suitable anode material for high-power lithium ion capacitors.

4. Conclusion

In this work, a light and binder-free bilayer fabric electrode composed of silicon nanowires and copper nanowires for lithium-ion capacitors (LICs) is reported. This fabric electrode exhibits a high specific capacity of 2800 mA h g^{-1} and excellent cycling stability after 50 cycles, showing good potential as the anode of LICs. The LICs we proposed employed pre-lithiated silicon/copper nanowire fabric and activated carbon as the anode and the cathode, respectively. Moreover, cases involving various mass ratios of silicon to active carbon were investigated to determine the optimal ratio that leads to the best compromise of energy density and power density of LICs. These LICs showed remarkable performance with a specific capacitance of

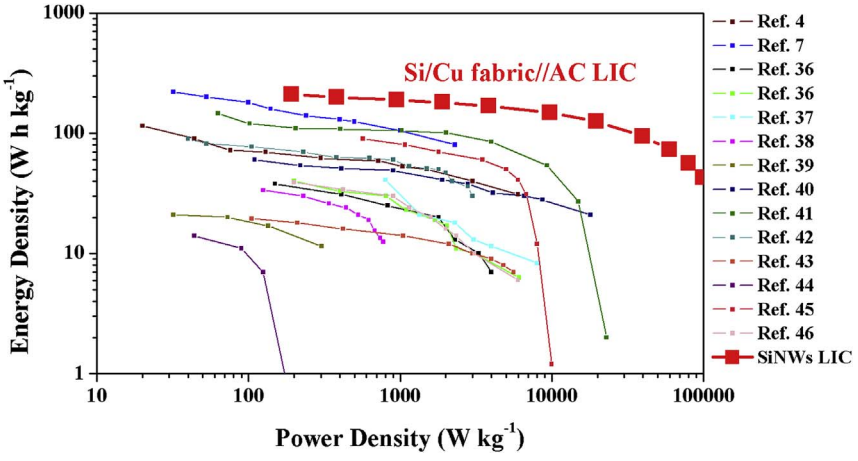

Fig. 7. Ragone plot of Si/Cu fabric//AC lithium ion capacitor along with other reported lithium ion capacitors [4,7,37–47].

Table 1
Electrochemical performances of various LICs.

Hybrid System (anode//cathode)	Voltage Window	Cathode Loading Mass (mg)	Current Density ($A\ g^{-1}$)	Energy Density ($W\ h\ kg^{-1}$)	Power Density ($W\ kg^{-1}$)	Ref.
Lithium ion capacitors						
AC//$LiNi_{0.5}Mn_{1.5}O_4$	1-3 V	11.3	0.3	56	~600	[12]
AC//$LiNi_{0.5}Mn_{1.5}O_4$	1.5–2.8 V	–	1	55	~2200	[11]
$LiNi_{0.5}Mn_{1.5}O_4$//AC	1.5–3.25 V	8.5	1.5	20	3300	[34]
MnO_2/CNT//$LiMn_2O_4$	1.6–4.1 V	1.1	1.95	26	2400	[14]
graphite//AC	1.5–5 V	2–6	0.65	60–90	10,000	[42]
CNT/V_2O_5//AC	0.1–2.7 V	3–5	0.13	20–40	20,000	[47]
LTO/AC//AC	0.5–3.5 V	–	4	90–32	6000	[4]
AC//Graphene-NiCo	0-1.4 V	30	30	19.5	5600	[44]
$LiTi_2(PO_4)_3$//AC	0-3 V	12.7	0.03	14	180	[45]
TiO_2/RGO//AC	1-3 V	–	4	10–42	~10,000	[38]
TiO_2/CNT//AC	1-3 V	1.5–2	15	30–120	12,000	[41]
$H_2Ti_6O_{13}$ NWs//mesoporous carbon	1-3.5 V	2	10	90	11,000	[46]
Fe_3O_4/Graphene//3DGraphene	1-4 V	6.75	2	60–90	~2500	[7]
Graphene/LTO//3DGraphene	0-3 V	–	11.17	95	~3000	[43]
LTO//AC	1-3 V	–	1.5	22–28	~3000	[49]
3D-MNO/CNS//CNS	1-4 V	–	5	90–180	15,000	[50]
graphene//AC	2-4 V	3	0.4	100	222	[31]
NbN/N graphene//AC	2-4 V	–	0.5	122	2000	[51]
graphdiyne//AC	2-4 V	–	0.5	100	1000	[52]
B-Si/SiO_2/C//PSC	2–4.5	4	3.2	128	9704	[23]
Si/Cu fabric//AC	1.5–4.2 V	0.8	50	210	99,000	our work

$156\ F\ g^{-1}$ at $0.1\ A\ g^{-1}$, which was approximately twice of that of activated carbon in electric double-layer high current density. This Si/Cu fabric//AC LIC shows good cycling stability with a fine retention of 54% after 1500 cycles when cycled at $5\ A\ g^{-1}$, and the cycling performance is enhanced greatly when the mass ratio of AC/silicon is decreased from 2 to 0.32, resulting in a higher retention of 90% with an extremely more lasting cycle life of 30,000 cycles when cycled at an even higher current density of $10\ A\ g^{-1}$. At a low power density of $193\ W\ kg^{-1}$, the Si/Cu fabric//AC LIC can achieve high energy density of $210\ W\ h\ kg^{-1}$. As the power density is increased to $99\ kW\ kg^{-1}$, the energy density still remains at $43\ W\ h\ kg^{-1}$, showing the excellent rate performance. Hence, the bilayer Si/Cu nanowire fabric is a perfectly suitable anode material for high power lithium ion capacitors. This LIC having working voltage window from 1.5 V to 4.2 V can light up green LED bulbs and provide higher voltage and better energy density than supercapacitors, which fails to turn on those green LED bulbs, indicating various applications of LICs. In future research, there must be effort put in the factors concerning the cycling durability, including the stability of AC and the influence of volumetric expansion upon lithiation and delithiation of Si nanowires, to further assemble the pouch cell of Si/Cu fabric//AC to obtain an even higher capacitance to be used in more applications, such as EV and HEV.

Acknowledgments

We acknowledge the financial support by the Ministry of Science and Technology, Taiwan through the grants of NSC 102-2221-E-007-023-MY3, MOST 103-2221-E-007-089-MY3, MOST 103-2622-E-007-025, and MOST 102 − 2633-*M*-007-002.

Appendix A. Supplementary data

Supplementary data related to this article can be found at http://dx.doi.org/10.1016/j.jpowsour.2018.01.046.

Basic characterization of the silicon or copper nanowires including SEM images, TEM images, EDS results, and XRD patterns are shown in supporting information; Cycling life and the voltage profiles of Si/Cu nanowires bilayer fabric lithium ion batteries (LIBs) at different current densities; the voltage profiles of Si/Cu nanowires bilayer fabric lithium ion capacitors (LICs) at different current densities. This material is available free of charge *via* the Internet at http://pubs.acs.org.

References

[1] J.R. Miller, P. Simon, Science 321 (5889) (2008) 651–652.
[2] P. Simon, Y. Gogotsi, Nat. Mater. 7 (11) (2008) 845–854.
[3] P. Simon, Y. Gogotsi, B. Dunn, Science 343 (6176) (2014) 1210–1211.
[4] H.S. Choi, J.H. Im, T. Kim, J.H. Park, C.R. Park, J. Mater. Chem. 22 (33) (2012) 16986–16993.
[5] I. Plitz, A. DuPasquier, F. Badway, J. Gural, N. Pereira, A. Gmitter, G.G. Amatucci, Appl. Phys. A 82 (4) (2006) 615–626.
[6] S.R. Sivakkumar, A.G. Pandolfo, Electrochim. Acta 65 (2012) 280–287.
[7] F. Zhang, T. Zhang, X. Yang, L. Zhang, K. Leng, Y. Huang, Y. Chen, Energy Environ. Sci. 6 (5) (2013) 1623–1632.
[8] E. Frackowiak, F. Béguin, Carbon 39 (6) (2001) 937–950.
[9] L.L. Zhang, X.S. Zhao, Chem. Soc. Rev. 38 (9) (2009) 2520–2531.
[10] S.R.C. Vivekchand, C.S. Rout, K.S. Subrahmanyam, A. Govindaraj, C.N.R. Rao, J. Chem. Sci. 120 (1) (2008) 9–13.
[11] H. Li, L. Cheng, Y. Xia, Electrochem. Solid State Lett. 8 (9) (2005) A433–A436.
[12] H. Wu, C.V. Rao, B. Rambabu, Mater. Chem. Phys. 116 (2–3) (2009) 532–535.
[13] X.-L. Wu, L.-Y. Jiang, F.-F. Cao, Y.-G. Guo, L.-J. Wan, Adv. Mater. 21 (25–26) (2009) 2710–2714.
[14] S.-B. Ma, K.-W. Nam, W.-S. Yoon, X.-Q. Yang, K.-Y. Ahn, K.-H. Oh, K.-B. Kim, Electrochem. Commun. 9 (12) (2007) 2807–2811.
[15] G.G. Amatucci, F. Badway, A. Du Pasquier, T. Zheng, J. Electrochem. Soc. 148 (8) (2001) A930–A939.
[16] A.D. Pasquier, I. Plitz, J. Gural, S. Menocal, G. Amatucci, J. Power Sources 113 (1) (2003) 62–71.
[17] W.J. Weydanz, M. Wohlfahrt-Mehrens, R.A. Huggins, J. Power Sources 81–82 (1999) 237–242.
[18] C.K. Chan, H. Peng, G. Liu, K. McIlwrath, X.F. Zhang, R.A. Huggins, Y. Cui, Nat. Nanotechnol. 3 (1) (2008) 31–35.
[19] M.N. Obrovac, L. Christensen, Electrochem. Solid State Lett. 7 (5) (2004) A93–A96.
[20] L. Lin, Y. Ma, Q. Xie, L. Wang, Q. Zhang, D.-L. Peng, ACS Nano 11 (7) (2017) 6893–6903.
[21] J.K. Lee, K.B. Smith, C.M. Hayner, H.H. Kung, Chem. Commun. (J. Chem. Soc. Sect. D) 46 (12) (2010) 2025–2027.
[22] K. Kang, H.-S. Lee, D.-W. Han, G.-S. Kim, D. Lee, G. Lee, Y.-M. Kang, M.-H. Jo, Appl. Phys. Lett. 96 (5) (2010) 053110.
[23] R. Yi, S. Chen, J. Song, M.L. Gordin, A. Manivannan, D. Wang, Adv. Funct. Mater. 24 (47) (2014) 7433–7439.
[24] D.S. Gardner, C.W. Holzwarth Iii, Y. Liu, S.B. Clendenning, W. Jin, B.-K. Moon, C. Pint, Z. Chen, E.C. Hannah, C. Chen, C. Wang, E. Mäkilä, R. Chen, T. Aldridge, J.L. Gustafson, Nano Energy 25 (2016) 68–79.
[25] S. Barth, M.S. Seifner, J. Bernardi, Chem. Commun. (J. Chem. Soc. Sect. D) 51 (61) (2015) 12282–12285.
[26] F.-W. Yuan, H.-Y. Tuan, Chem. Mater. 26 (6) (2014) 2172–2179.
[27] V.C. Holmberg, B.A. Korgel, Chem. Mater. 22 (12) (2010) 3698–3703.
[28] H.-Y. Tuan, B.A. Korgel, Chem. Mater. 20 (4) (2008) 1239–1241.

[29] T.D. Bogart, D. Oka, X. Lu, M. Gu, C. Wang, B.A. Korgel, ACS Nano 8 (1) (2014) 915–922.
[30] H.-J. Yang, S.-Y. He, H.-Y. Tuan, Langmuir 30 (2) (2014) 602–610.
[31] J.J. Ren, L.W. Su, X. Qin, M. Yang, J.P. Wei, Z. Zhou, P.W. Shen, J. Power Sources 264 (2014) 108–113.
[32] H. Wang, Y. Zhang, H. Ang, Y. Zhang, H.T. Tan, Y. Zhang, Y. Guo, J.B. Franklin, X.L. Wu, M. Srinivasan, H.J. Fan, Q. Yan, Adv. Funct. Mater. 26 (18) (2016) 3082–3093.
[33] Z. Fan, J. Yan, T. Wei, L. Zhi, G. Ning, T. Li, F. Wei, Adv. Funct. Mater. 21 (12) (2011) 2366–2375.
[34] N. Arun, A. Jain, V. Aravindan, S. Jayaraman, W. Chui Ling, M.P. Srinivasan, S. Madhavi, Nanomater. Energy 12 (2015) 69–75.
[35] H. Wang, D. Mitlin, J. Ding, Z. Li, K. Cui, J. Mater. Chem. 4 (14) (2016) 5149–5158.
[36] H. Li, L. Peng, Y. Zhu, X. Zhang, G. Yu, Nano Lett. 16 (9) (2016) 5938–5943.
[37] Z. Chen, V. Augustyn, X. Jia, Q. Xiao, B. Dunn, Y. Lu, ACS Nano 6 (5) (2012) 4319–4327.
[38] H. Kim, M.-Y. Cho, M.-H. Kim, K.-Y. Park, H. Gwon, Y. Lee, K.C. Roh, K. Kang, Adv. Eng. Mater. 3 (11) (2013) 1500–1506.
[39] J. Yin, L. Qi, H. Wang, ACS Appl. Mater. Interfaces 4 (5) (2012) 2762–2768.
[40] R. Ding, L. Qi, H. Wang, Electrochim. Acta 114 (2013) 726–735.
[41] Z. Chen, Y. Yuan, H. Zhou, X. Wang, Z. Gan, F. Wang, Y. Lu, Adv. Mater. 26 (2) (2014) 339–345.
[42] V. Khomenko, E. Raymundo-Piñero, F. Béguin, J. Power Sources 177 (2) (2008) 643–651.
[43] K. Leng, F. Zhang, L. Zhang, T. Zhang, Y. Wu, Y. Lu, Y. Huang, Y. Chen, Nano Rev. 6 (8) (2013) 581–592.
[44] H. Wang, C.M.B. Holt, Z. Li, X. Tan, B.S. Amirkhiz, Z. Xu, B.C. Olsen, T. Stephenson, D. Mitlin, Nano Rev. 5 (9) (2012) 605–617.
[45] V. Aravindan, W. Chuiling, M.V. Reddy, G.V.S. Rao, B.V.R. Chowdari, S. Madhavi, Phys. Chem. Chem. Phys. 14 (16) (2012) 5808–5814.
[46] Y. Wang, Z. Hong, M. Wei, Y. Xia, Adv. Funct. Mater. 22 (24) (2012) 5185–5193.
[47] Z. Chen, V. Augustyn, J. Wen, Y. Zhang, M. Shen, B. Dunn, Y. Lu, Adv. Mater. 23 (6) (2011) 791–795.
[48] W.-C. Chang, T.-L. Kao, Y. Lin, H.-Y. Tuan, J. Mater. Chem. A 5 (2017) 22662–22671.
[49] A. Jain, V. Aravindan, S. Jayaraman, P.S. Kumar, R. Balasubramanian, S. Ramakrishna, S. Madhavi, M.P. Srinivasan, Sci. Rep. 3 (2013) 3002.
[50] H. Wang, Z. Xu, Z. Li, K. Cui, J. Ding, A. Kohandehghan, X. Tan, B. Zahiri, B.C. Olsen, C.M.B. Holt, D. Mitlin, Nano Lett. 14 (4) (2014) 1987–1994.
[51] M. Liu, L. Zhang, P. Han, X. Han, H. Du, X. Yue, Z. Zhang, H. Zhang, G. Cui, Part. Part. Syst. Char. 32 (11) (2015) 1006–1011.
[52] H. Du, H. Yang, C. Huang, J. He, H. Liu, Y. Li, Nanomater. Energy 22 (2016) 615–622.